Acta Cryst. (1993). D**49**, 120–128

Towards the Measurement of Ideal Data for Macromolecular Crystallography using Synchrotron Sources

BY J. R. HELLIWELL

Department of Chemistry, University of Manchester, Oxford Road, Manchester M13 9PL, England, and SERC Daresbury Laboratory, Daresbury, Warrington WA4 4AD, England

S. EALICK

Section of Biochemistry and Cornell High Energy Synchrotron Source, Cornell University, Ithaca, New York, USA

AND P. DOING, T. IRVING AND M. SZEBENYI

Cornell High Energy Synchrotron Source, Cornell University, Ithaca, New York, USA

This paper is dedicated to Professor M. M. Woolfson FRS, University of York, on the occasion of his 65th birthday, who would remark to the author 'Our new direct method works with ideal protein crystal data but not with real data'

(*Received* 27 *April* 1992; *accepted* 24 *June* 1992)

Abstract

Synchrotron radiation has been used extensively to overcome a variety of technical challenges involved in data collection from macromolecular crystals. The next generation of such sources offer a higher brilliance at much shorter wavelengths than hitherto available. Hence, the quality of X-ray diffraction data from crystals of biological macromolecules will be further improved in terms of reduced systematic and random errors, in conjunction with a very high degree of completeness of, and multiple measurements within, the data set. Real data sets should be able to approach closely the quality of ideal data sets. Tests at CHESS are described of the feasibility of recording protein crystal diffraction patterns at ultra-short wavelengths ($\lambda = 0.3$ Å) and very-short wavelengths ($\lambda = 0.5$ Å), in monochromatic rotating crystal geometry.

1. Introduction

Short-wavelength monochromatized beams have been very effective in macromolecular crystal data collection at sources such as the Daresbury SRS, particularly from viruses. Crystal absorption errors have been reduced and crystal lifetimes improved. The use of 0.9 Å wavelength maximized the absorption of photographic film as detector, due to the Br *K* edge, in a wavelength region favourable to the sample. Also, it is where the Daresbury Wiggler emission peaked ($\lambda_c = 0.9$ Å).* The next generation of synchrotron sources, such as the European Synchrotron Radiation Facility (ESRF), offer copious fluxes at even shorter photon wavelengths. Detectors such as the image plate, which contains barium (*K*-edge $\lambda = 0.331$ Å) and caesium iodide scintillators coupled to charge-coupled devices (N. M. Allinson & K. Moon, personal communication), offer optimal detection strategies in an even shorter wavelength regime. Systematic errors of the measurement can be essentially eliminated as well as crystal lifetime improved so that multiple measurements can be made, random errors minimized and near 100% data completeness realized. The reduction in scattering efficiency with these shorter wavelengths is compensated for by the increase in intensity of an SR source like the ESRF in that range. The required long crystal-to-detector distances can be tolerated because of the collimation offered by the tight divergence of the beam in the horizontal as well as the vertical by an undulator and even by the multipole wiggler. The perfection of macromolecular crystals, with mosaic spreads in the range of 0.02° (0.3 mrad) will permit exploitation of these ultra-short wavelengths and fine beam collimation. The future expectations for the quality of native data could not be better and offer an exciting prospect for phasing by direct methods and improved model refinement. A survey of work in macromolecular crystallography with synchrotron radiation can be found in Helliwell (1992). In this paper aspects of monochromatic data collection are discussed whereby the production and use of an ultra-short wavelength, such as 0.33 Å, of the required incident flux, collimation and focused spot size at the sample, can be addressed. Aspects to be

* λ_c is the critical wavelength of the synchrotron radiation emission curve.

0907-4449/93/010120-09$06.00

considered include the diffracted beam energy for a given *hkl* and the parameters on which this depends, instrument smearing effects and diffraction-spot angular reflecting ranges, Lorentz and polarization effects, the absorption of X-rays, and radiation damage and sample heating (particularly as a function of wavelength). Preliminary results are given of experiments at CHESS with an unfocused, monochromatized beam on station F2, fed by a 24-pole multipole wiggler, firstly at a wavelength of 0.5 Å and then at 0.3 Å using a lysozyme crystal as a test sample. Finally, in the *Appendix*, possible instrument configurations are explored for the production and detection of ultra-short wavelengths in the context of machines like ESRF, but also pertinent to APS, SPRING-8, PETRA, TRISTAN *etc.*, as well as existing high-energy machines such as CHESS.

2. Background information

2.1. *Diffracted beam energy (monochromatic/rotating crystal method)*

The total energy in a diffracted beam from a particular reflecting plane (*hkl*) for a crystal rotating with constant angular velocity ω through the reflecting position is, in the kinematical regime,

$$E(hkl) = (e^4/m^2c^4\omega)I_0\lambda^3 LPA(V_x/V_0^2)|\mathbf{F(h)}|^2 \quad (1)$$

where I_0 is the intensity of the incident X-ray beam of wavelength λ, P is the correction for polarization, L is the Lorentz-factor correction for the relative time spent by the reciprocal lattice points in the reflecting position, A is a correction for absorption of the sample (P, L and A are different for each reflection), V_x is the volume of the crystal sample, V_0 is the volume of the unit cell and $|\mathbf{F(h)}|$ is the structure-factor amplitude. It is most important to note that the Lorentz factor is essentially proportional to $1/\sin\theta$, *i.e.* to $1/\lambda$ and therefore $E(hkl)$ is proportional to λ^2 when this is taken into account.

2.2. *Intrinsic rocking width, mosaic spread and reflecting range*

An ideally imperfect crystal, for which (1) holds, is defined as being made up of many small blocks randomly misaligned with respect to each other. Each block is perfectly crystalline and has an intrinsic rocking width, η_{hkl}, owing to the non-infinite number of unit cells contributing to the block. An expression for η_{hkl} is derivable from the dynamical theory of X-ray diffraction (Zachariasen, 1945), as (given in SI units):

$$\eta_{hkl} = \frac{1}{\pi^2\varepsilon_0}\frac{d^2e^2}{mc^2}\frac{\tan\theta_B}{V_0}|\mathbf{F(h)}| \quad (2)$$

where d is the interplanar spacing for a particular Bragg plane, θ_B the Bragg angle, V_0 is the unit-cell volume and $|\mathbf{F(h)}|$ the structure amplitude.

Calculations using (2) for a 100 Å unit cell protein crystal indicate a few arc seconds for η_{hkl} (Helliwell, 1988). In fact, if a perfect protein crystal existed *i.e.* its mosaic block size was the whole crystal size, the scattering would still be in the weak regime. With such a limit, dynamical theory is not needed and the kinematical theory applies. In general though protein crystals are referred to as mosaic.

The blocks making up a 'mosaic' crystal in the model of an ideally imperfect crystal are slightly misaligned in angle with respect to one another. The overall angular misalignment is the so-called mosaic spread, η, intrinsic to the crystal sample and where $\eta > \eta_{hkl}$. Typical values of η are 0.1° for a protein crystal, but at the synchrotron values as small as 0.01–0.02° for η for particular crystals have been observed (Colapietro, Cappuccio, Marciante, Pifferi, Spagna & Helliwell, 1992). Less well ordered samples have η's in the range 0.5–1.0° or even larger.

The reflecting range, φ_R, measured for a given reflection, ignoring η_{hkl} above as a very small effect, is determined by η, as well as the X-ray beam divergence angles and spectral bandwidth. Additionally, φ_R is a function of the reciprocal coordinates of a given reciprocal lattice point. φ_R increases gradually with increasing θ (due to the effect of spectral smearing) and dramatically the nearer the reciprocal lattice point is to the rotation axis (becoming infinite on the axis). The actual expression for φ_R depends on the instrument (*i.e.* the X-ray beam parameters) and on the diffraction geometry.

Greenhough & Helliwell (1982*b*) produced a theory for the general setting of an instrument based on the bent triangular monochromator (Fig. 1). The angular reflecting range φ_R for the protein crystal sample is given, in the case of a horizontal rotation axis (the most common), by

$$|\varphi_R| \simeq [L^2(\delta d^{*2} + \gamma_H)^2 + \gamma_v^2]^{1/2} + 2\varepsilon_s L \quad (3)$$

where L is the Lorentz factor, γ_H and γ_v are the incoming horizontal and vertical cross-fire angles at the sample, δ is $\frac{1}{2}(\delta\lambda/\lambda)_{corr}$, d^* is the reciprocal planar distance and ε_s is given by

$$\varepsilon_s = \frac{d^*\cos\theta_{hkl}}{2}[\eta + (\delta\lambda/\lambda)_{conv}\tan\theta_{hkl}] \quad (4)$$

where η is the mosaic spread and $(\delta\lambda/\lambda)_{conv}$ is given by $\eta_{diff}^{mono}\cot\theta_{mono}$ (Greenhough & Helliwell, 1982*a*,*b*), η_{diff}^{mono} being the monochromator rocking width.

2.3. *Absorption of X-rays*

An X-ray beam passing through a sample suffers absorption and its intensity is attenuated. The

absorbed X-rays cause thermal heating and radiation damage. In macromolecular crystallography this often necessitates the use of more than one crystal to collect a complete data set. The derivation of $|\mathbf{F(h)}|$ from $E(hkl)$ requires an absorption correction to be applied; the simplest situation is for the case of a spherical crystal (without a capillary) completely bathed in a uniform X-ray beam. In such a case all the reflections would be equally reduced in intensity. The situation of such a spherical crystal almost never exists in macromolecular crystallography.

For a beam of monochromatic X-rays passing through an isotropic material the transmitted beam has intensity

$$I = I_0 \exp(-\mu x) \tag{5}$$

where I_0 is the incident intensity, μ is the linear absorption coefficent and x is the path length through the sample. For a sample consisting of a number of elements N, the overall mass absorption coefficent μ_m is given by,

$$\mu_m = \sum_{i=1}^{N} g_i(\mu_m)_i \tag{6}$$

where g_i is the mass fraction and $(\mu_m)_i$ the mass absorption coefficient of the ith element, and

$$\mu = \rho \mu_m \tag{7}$$

where ρ is the density. Usually, ρ is expressed in g cm^{-3}, μ_m in cm^2 g^{-1} and hence μ in cm^{-1} (although mm^{-1} is common). Values of μ_m between 0.1 and 2.89 Å wavelengths are tabulated for the elements (Li to Bi, U) by Sasaki (1990). Values of μ_m at wavelengths of 0.33, 0.9 and 1.488 Å, kindly calculated by Sasaki, along with ρ values, are tabulated in Helliwell (1992).

The mass absorption coefficient μ_m varies with wavelength according to the following relationship, in the absence of elemental absorption edges,

$$\mu_m = a\lambda^3 + b\lambda^4 \tag{8}$$

where a and b are constants of proportionality. This is the so-called Victoreen relationship and is dominated primarily by the λ^3 term. There are discontinuities in the wavelength dependency that occur at elemental absorption edges.

The effect of absorption on the reflection intensities is obviously to reduce them; in the absence of a correction this would affect the estimation of individual atomic temperature factors in molecular model refinement. The absorption corrections applied to individual reflections are different from one to another being θ and ψ dependent. In the case where a single data set is obtained from several crystals each of variable size and shape, then the lack of an absorption correction will leave systematic

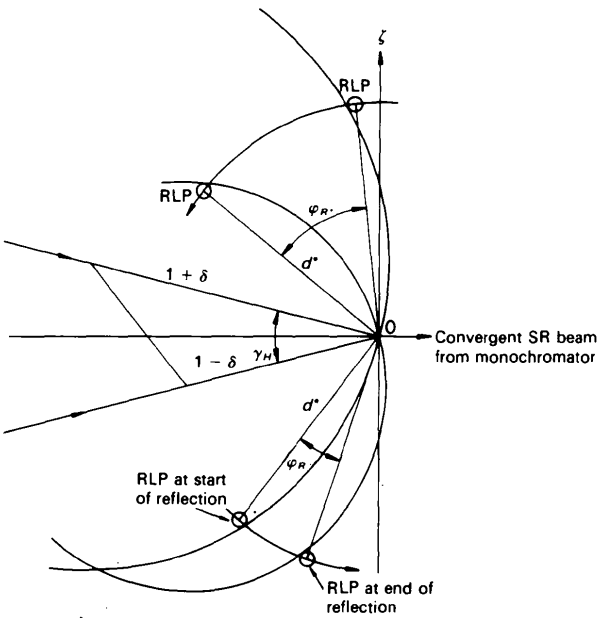

Fig. 1. Prediction of partiality and angular reflecting range of a given reciprocal lattice point (RLP). One of the most commonly used instruments so far for monochromatic data collection is that based on the bent triangular monochromator. In its general setting the beam convergence angle γ_H has associated with it a 'correlated' $\delta\lambda/\lambda$ term shown here as $\delta = \frac{1}{2}(\delta\lambda/\lambda)_{corr}$. Usually the instrument is set at the Guinier setting for which $\delta = 0$ or γ_H is limited in value (by slits) to reduce the value of δ to ~ 0.001. The RLP is not actually a 'point' but is finite in size because of sample mosaic spread. A given hkl plane is therefore in the reflecting position, not just instantaneously, but over an angle φ_R. The figure here is based on the Ewald construction and shows two RLP's, in the zero level, both at d^* from the origin of reciprocal space but on opposite sides ($\pm\zeta$) of the beam with reflecting ranges φ_{R^+} and φ_{R^-}. For clarity, a vertical rotation axis, rather than a horizontal axis, is shown. After Greenhough & Helliwell (1982*b*).

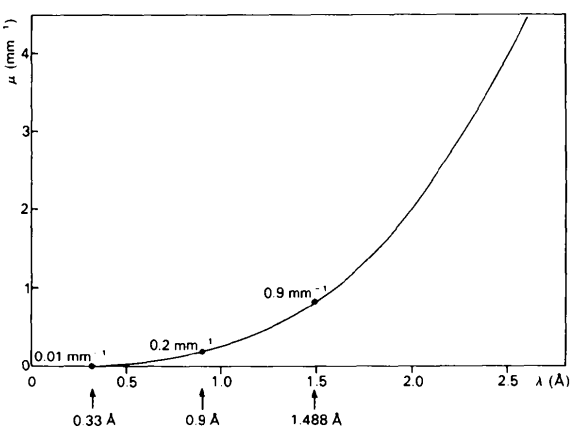

Fig. 2. The variation of linear absorption coefficient with wavelength for a protein crystal. The wavelengths marked are those typically used for rotine data collection at synchrotron radiation sources (*e.g.* 1.488 Å at station 7.2 of the SRS, 0.9 Å at station 9.6 of the SRS) and 0.33 Å as a future standard wavelength. After Helliwell (1992).

Table 1. *Results of the model calculations [based on Helliwell (1992)]*

The calculations suggest that shorter wavelengths increase the amount of data that can be recorded per crystal at room temperature. These calculations actually underestimate the benefit if $\varepsilon = 5$ is used for all intensities. Note that (*a*) a typical protein crystal sample of size 0.1 × 0.1 × 0.1 mm is assumed and 100 Å unit cell; (*b*) ε may well be less at the higher intensity levels rather than the constant value of 5 assumed in this table; (*c*) an identical absorption efficiency (100%) of the detector is assumed in these calculations for 0.33, 0.5 and 1.5 Å wavelengths. Hence, to truly exploit these benefits of changing wavelengths needs an efficient detector in each wavelength range. For example, at 0.9 Å film is 40% efficient and the image plate 80% efficient, whereas at 0.33 Å wavelength, film is only 8% efficient in absorbing photons whereas the image plate is 44% efficient. ε is a damage factor *i.e.* an absorbed photon will damage a certain number of protein molecules (Blake & Phillips, 1962). Exposure times are given for a typical resolution limit of 2 Å.

Example source/ beamline	Wavelength of the beam (Å)	Intensity at the sample (photons $s^{-1} mm^{-2}$)	Absorbed heat $\delta H/\delta t$ (W)	Adiabatic temperature rise $\delta T/\delta t$ ($K\ s^{-1}$)	Radiation lifetime $\varepsilon\tau$ (s)	Typical exposure time per angular degree (s)	Angular degrees of data per sample (if $\varepsilon = 5$) (°)
SRS station 7.2	1.5	10^{11}	1.19×10^{-7}	0.028	11000	100	22
SRS station 9.6	0.9	10^{11}	4.4×10^{-8}	0.01	5000	278*	36
	1.5	10^{14}	1.19×10^{-4}	28	11	0.1	22
ESRF multipole wiggler	0.5	10^{14}	1.31×10^{-5}	3.1	303	0.9*	67
ESRF undulator	0.33	10^{14}	6.0×10^{-6}	1.4	1000	2.0*	100

* Due allowance has been made for the difference in scattering efficiency of the sample at these wavelengths.

errors in the data. Even when a single crystal is used for a complete native data set and an identically shaped and mounted crystal is used as the heavy-atom derivative, the lack of an absorption correction can leave large discrepancies between measured and calculated isomorphous or anomalous differences. In addition, an incorrectly applied absorption correction can exacerbate systematic errors.

The range of the magnitudes of the absorption correction that have to be applied to a protein crystal for Cu $K\alpha$ wavelength can be estimated, based on a μ value of $\sim 1\ mm^{-1}$ and crystals up to 1 mm thick, from equation (5). For comparison, at a shorter wavelength 0.9 Å, μ is reduced to $0.2\ mm^{-1}$ and at 0.33 Å, $0.01\ mm^{-1}$. Clearly, the absolute and relative absorption effects decrease considerably for the shorter wavelength examples (see Fig. 2).

2.4. *Radiation damage and sample heating*

Radiation damage and sample heating arise from the absorption of X-rays in the sample. The sensitivity of the specimen to these effects depends markedly on the temperature of the specimen. Comments will be restricted to room or near room temperature where proteins maintain the solvent channels going through the crystal as liquid.

Ionization processes occur producing free radicals. They are damaging to biological macromolecules. Free radicals have a natural diffusion rate and, hence, radiation damage is dose and rate dependent, *i.e.* a larger total dose can be tolerated by a sample if that dose is delivered at a higher rate.

Sample heating in SR beams was introduced as a consideration by Stuhrmann (1978). Helliwell & Fourme (1983) considered radiation damage and sample heating in evaluating the usefulness of the prospective fluxes at the specimen that might be anticipated using the ESRF. Helliwell & Fourme (1983) and Helliwell (1984, pp. 1470–1473) discussed the need to go to shorter X-ray wavelengths (*e.g.* 0.5 instead of 1.5 Å), to reduce the fraction of absorbed photons, and to use cryotemperatures, with frozen crystals mounted on a copper fibre, to limit the temperature rise experienced by the sample. In this way, frozen microcrystals of proteins of size $\sim 10\ \mu m$ could be successfully studied on the ESRF. This application of the ESRF was discussed further in Helliwell (1989).

Cryocrystallography of biological macromolecules has been developed by Hope (1988) as a generally applicable method. A striking success has been its use in ribosome crystal structure studies. Hope (1988) has observed that improvements in diffraction pattern lifetimes of at least 1000-fold can be obtained by cooling crystals to liquid-nitrogen temperature. Henderson (1990) has compared the behaviour of frozen protein crystals in X-ray *versus* electron beams; the central conclusion of this paper is as follows. Henderson (1990) predicts that, 'however low the temperature of the specimen, X-ray doses of about 2×10^7 Grays (1 Gray = 100 rad) will always destroy the crystalline diffraction from protein crystals'.

Doubts exist about how widely applicable the use of cryotechniques will be for X-ray data collection. Often the mosaicity of the specimen is increased on freezing, which can lead to serious overlap of reflections owing to increased spot size and angular reflecting range. Whether this can be tolerated or not depends on the size of the unit cell. Hence, finding ways of curtailing radiation damage whilst continuing to operate at room temperature is important. The use of shorter and shorter wavelengths is tractable with more brilliant, *i.e.* finely focused, high-flux, more-collimated beams. These methods rely on the intrinsic perfection of a given protein crystal (Colapietro *et al.*, 1992) a property that is remarkable indeed.

Table 1 summarizes the results of some model calculations (Helliwell, 1992) for a range of intensities and at several different wavelengths. These

indicate an increase in the amount of data recordable per crystal at shorter wavelengths. If anything, these calculations underestimate the improvement factors. For example, use of an SRS bending magnet at 1.488 Å and the SRS wiggler beams at 0.9 Å wavelengths yields, for similar incident intensities, improvement factors in crystal lifetimes of 2–4 instead of 36/22 = 1.64; for example, with crystals of the virus SV40 a factor of four improvement was observed (Liddington, Yan, Moulai, Sahli, Benjamin & Harrison, 1991).

3. Use of short wavelengths in data collection

The positive benefits of using a short wavelength are several fold. The reduction in sample absorption (Fig. 2) has three benefits. Firstly, the high-resolution reflections especially are attenuated less than they would otherwise be, *i.e.* the overall temperature factor of the sample is less; this is important for macromolecular model refinement. Secondly, sample to sample variations in absorption are reduced; this improves data consistency (reducing merging R's) and improves the accuracy of the estimation of isomorphous and anomalous differences. Thirdly, as we have seen in Table 1, the sample lifetime is enhanced, although this effect depends to some extent on an individual sample's sensitivity to radiation. Additionally, the geometry of the diffraction, coupled with the collimation of the beam, allows longer crystal-to-detector/film distances to be used for a given resolution limit (d spacing). The signal-to-noise ratio of the measurement is thereby enhanced (Fig. 3).

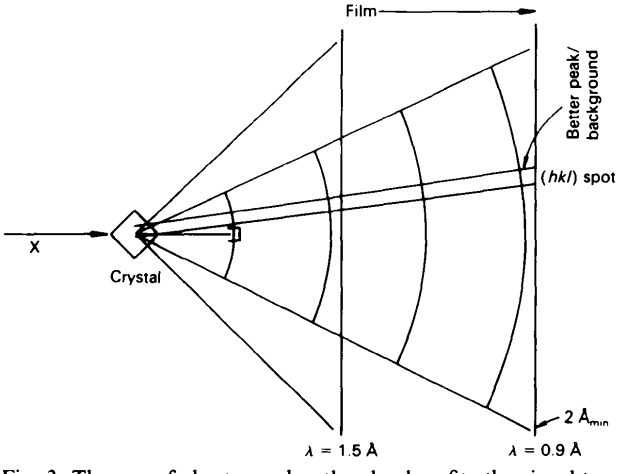

Fig. 3. The use of short wavelengths also benefits the signal-to-noise ratio of a diffraction-spot intensity measurement. The detector can be moved further from the crystal for a given resolution limit. As a result the background per unit area on the film is reduced according to the inverse square law, excluding the diffuse scattering. The diffraction spot hardly increases in size because of the beam collimation. The reduced scattering at short wavelengths [equation (1)] is compensated for by the strength of the synchrotron radiation beam intensity at the sample. After Helliwell (1992).

The penalty of using short-wavelength radiation is the reduction in the scattering efficiency of the sample. The wavelength-dependent factors in the Darwin formula are $\lambda^3 L$, where L is the Lorentz factor which varies approximately as $1/\lambda$. Hence, use of 0.9 Å instead of 1.54 Å reduces the scattering efficiency by a factor of $\sim$2.9 and use of 0.3 Å *further* reduces it by 9 (*i.e.* compared with 0.9 Å).

The absorption efficiency of the detector/film also reduces with wavelength according to a factor $\exp(-\mu t)$. Photographic film, for example, reduces in absorption efficiency between 1.54 and 0.9 Å by a factor of $\sim$1.35. However, for film the Br K edge at 0.92 Å and the silver bromide in the emulsion do allow specific enhancement of the absorption if a $\lambda \leq 0.92$ Å is chosen.

Experience with the television detector system (Enraf–Nonius FAST) on the focused wiggler beam line at Daresbury using a wavelength of 0.9 Å suggests that the intensity of the diffraction patterns is often somewhat too strong for the detector. Use of even shorter wavelengths than 0.9 Å will reduce the strength of the pattern whilst giving further reduction in absorption errors and enhanced sample lifetime in the beam, *etc.*, outlined above. At the insertion-device machines such as the ESRF and the APS an undulator with a fundamental in the 1.0 Å region is realistic and will provide exceptionally low divergence beams in this beneficial short wavelength regime. An even shorter wavelength than 1.0 Å would be attractive for the user but could be achieved only in higher harmonics of the undulator emission. Some possibilities are put forward in the next section. Table 2 provides a compilation of published structures based on short-wavelength ($\lambda \simeq$ 0.9 Å) data collection in macromolecular crystallography up to 1991.

4. Possible uses and first trials of very-short and ultra-short wavelengths in monochromatic data collection

The previous sections (§2 and §3) outlined the basis of using shorter wavelengths in reducing absorption errors and prolonging crystal sample lifetime. The calculations shown in Table 1 indicate that there is no optimum wavelength as such but that it is always better to work at shorter and shorter wavelengths. Helliwell & Fourme (1983) suggested the use of a multipole wiggler on the ESRF at a monochromatized wavelength of 0.5 Å, see Helliwell (1984, p. 1472). Such a wavelength one could define as very short in contrast to short ($\sim$0.9 Å) or ultra-short ($\sim$0.3 Å). Protein crystal data have been col-

Table 2. *Published protein and virus structures based on the use of short-wavelength* ($\lambda \simeq 0.9$ Å) *synchrotron radiation up to* 1991 [*adapted from Helliwell* (1992)]

Sample	SR source*	Detector	λ (Å)	Unit-cell parameters a (Å) α (°)	b (Å) β (°)	c (Å) γ (°)	Space group	Resolution limit (Å)	Reason for using SR†	Reference
Beef despentapeptide insulin	SRS	FAST‡	0.9	52.7	26.2 93.4	51.7	$C2$	1.3	HR	Holden in Glover *et al.* (1988)
Chloramphenicol acetyl transferase	SRS	Film	0.90	74.5 92.5			$R32$	1.75	HR	Leslie *et al.* (1988) and Leslie (1990)
FMDV	SRS	Film	0.9	345			$I23$	2.9	RRD, LUC	Acharya *et al.* (1989)
Glycogen phosphorylase b	SRS	Film	0.9	128.5		116.3	$P4_12_12$	1.9	RRD, RAE	Oikonomakos *et al.* (1987) and Sprang *et al.* (1988)
Spinach ribulose bisphosphate carboxylase (rubisco)	SRS	Film	0.87	157.2		201.3	$C222_1$	2.4	RRD	Andersson *et al.* (1989)
Rh. rubrum rubisco	SRS	Film	0.87	65.5	70.6 92.1	104.1	$P2_1$	1.7	HR	Andersson *et al.* (1989)
p21 (Val-12) ras oncogene protein	SSRL	Film	1.08	83.2		105.1	$P6_522$	2.2	HR	Tong *et al.* (1989)
B. cereus phospholipase C	SRS	Film	0.88	89.93		73.99	$P4_12_12$	1.5	HR	Hough *et al.* (1989)
R-state glycogen phosphorylase	SRS	Film	0.88	119.0	190.0 109.35	88.2	$P2_1$	2.8	Tetramer in asymmetric unit	Barford & Johnson (1989)
A. niger α-amylase	SRS	Film	0.9	81.1	98.3	138.0	$C222_1$	2.1	HR, RAE	Boel *et al.* (1990)
Partially oxygenated *T*-state haemoglobin	SRS	Film	1.0	95.8	97.8	65.5	$P2_12_12_1$	1.5	HR	Waller & Liddington (1990)
SV40 virus	SRS	Film	0.9	558			$I23$	3.8	RRD, LUC	Liddington *et al.* (1991)

* SRS, Daresbury Synchrotron Radiation Source; SSRL, Stanford Synchrotron Radiation Laboratory.

† HR, high-resolution study for model refinement; RRD, reduced radiation damage; LUC, large unit cell; RAE, reduced absorption error use of a short wavelength.

‡ FAST is a tradename of the Enraf Nonius television area detector.

lected at SRS wiggler station 9.6 (Helliwell, Papiz, Moore & Thompson, 1984; Helliwell *et al.*, 1986) with nitrogenase crystals by J. Bolin at 0.6 Å wavelength.

A promising application of multipole wigglers (at 0.5 Å) or undulators (*i.e.* a harmonic at ~0.3 Å) is to solve the problem of data collection from very radiation sensitive crystals. For example, in virus data collection with film several hundred crystals are needed for structure determination. Of course, once the basic structure is known, a greatly reduced amount of data and far fewer crystals are needed in drug binding (difference Fourier) studies.

A series of test experiments need to be made with these kinds of samples at these wavelengths, *i.e.* 0.5 Å ideally on a multipole wiggler and 0.3 Å ideally on an undulator (harmonic). The intensity of these beams will compensate for the increase in exposure time resulting from the λ^2 effect of the Darwin formula (§2.1). At 0.5 Å the absorption efficiency of an image plate is still reasonable (50%) and at 0.33 Å (37.5 keV) it is ~44%. The Ba *K* edge at 0.331 Å usefully enhances the stopping power of an image plate from 19% just above the edge to 44% just below it. By comparison photographic film (Kodak DEF) would only absorb 8% of the photons at 0.33 Å.

The crystal-to-image plate distances for 0.5 and 0.3 Å are, of course, increased. This is advantageous because of the inverse square law effect in reducing the background under the diffraction spot. However, a crystal-to-film distance of, say, 0.5 m with a 1 mrad divergence beam would lead to a sizeable increase in the diffraction spot size (*i.e.* by 0.5 mm). On an undulator, however, beam divergences are intrinsically ~0.1 mrad and so the spot size over a 0.5 m distance would only increase by 0.05 mm owing to this effect (Table 3). Mosaic spreads of specimens also need to be narrow but ~0.3 mrad is a quite reasonable expectation for these samples (Helliwell, 1988; Colapietro *et al.*, 1992).

The beautiful combination of properties of synchrotron radiation is so often what is important in making an experiment work. In this context the undulator harmonic would provide a very high intensity beam at ultra-short wavelength (0.3 Å) with a very small divergence beam.

Table 3. *Image plate detector distances from the crystal and spot sizes at* 0.5 *and* 0.33 Å *wavelength* [*adapted from Helliwell* (1992)]

αD is the product of the typical divergence angle (0.1 mrad undulator, 1 mrad multipole wiggler) and the crystal sample-to-plate distance. A protein crystal mosaicity in the 0.1 mrad (0.006°) range is required if the longer crystal-to-plate distances are to be realized. As documented by Helliwell (1988) and Colapietro *et al.* (1992), protein crystals at room temperature do have rocking widths of 0.01–0.02° (0.17–0.34 mrad) FWHM.

	λ (Å)	d_{min} (Å)	θ (°)	IP radius (cm)	D (cm)	αD (mm)
Very-short wavelength (multipole wiggler)	0.5	3.0	4.780	10	59.4	0.59
	0.5	2.0	7.181	10	39.1	0.39
	0.5	1.5	9.594	10	28.7	0.29
	0.5	1.2	12.025	10	22.4	0.22
	0.5	1.0	14.478	10	18.1	0.18
Ultra-short wavelength (undulator harmonic)	0.33	3.0	3.153	10	90.5	0.091
	0.33	2.0	4.732	10	60.0	0.06
	0.33	1.5	6.315	10	44.6	0.045
	0.33	1.2	7.903	10	35.3	0.035
	0.33	1.0	9.497	10	29.1	0.029

The first tests at these sort of wavelengths are reported in this paper. At CHESS we have used a 24-pole multipole wiggler (critical wavelength 0.5 Å) and a monochromatized beam on station F2 to record oscillation exposures, $\Delta\varphi = 1°$, from a protein crystal (lysozyme) on Fuji imaging plates. Exposure times with this unfocused beam at $\lambda = 0.5$ Å were 10 min per degree and at $\lambda = 0.3$ Å, 25 min per degree (see Figs. 4*a* and 4*b* respectively). The plates were digitized on a Kodak prototype scanner at CHESS. The value of $R_{\rm merge}(I)$ for two identical exposures recorded at $\lambda = 0.32$ Å was 2.1% for data up to 1.7 Å resolution. The strongest reflections had R factors in the range 0.4–2.1%. The flux at the sample for this unfocused beam through a 0.3 mm collimator was estimated to be 2×10^9 photons s^{-1} at 0.5 Å and 7×10^8 photons s^{-1} at 0.3 Å with CHESS operating at 50 mA.

5. Concluding remarks

Ten years ago it would have seemed inconceivable that the structure of viruses would be solved using data collected at short wavelengths like 0.9 Å. After all, in the home laboratory Mo $K\alpha$ (0.71 Å) is reserved solely for unit cells up to ~20 Å and Cu $K\alpha$ (1.54 Å) for macromolecules. Yet 0.9 Å data collection on today's bending magnets and wigglers is commonplace. It is not unreasonable to consider routine data collection from radiation-sensitive samples like virus crystals, in future, using an undulator harmonic at 0.33 Å with an image plate placed 0.5–1.0 m from the crystal. Also, the high brilliance at short wavelengths (0.15 Å) of the higher harmonics from X-ray undulators would allow X-ray diffraction from macromolecular crystals almost totally free of absorption errors whilst stimulating the *K-edge* anomalous dispersion of high atomic number elements (*e.g.* mercury, platinum, *etc*).

Most importantly, native protein crystal data sets could be measured at wavelengths as short as 0.33 Å and which would also be free of absorption errors and with greatly reduced random errors. This would be due to the ability to have prolonged exposure times and repeated measurements before the protein crystal suffers radiation damage. Hence unprecedented data quality will be achieved, and maybe even improvements to atomic resolution of the diffraction data for protein crystals, might arise. These advantages could be combined with statistical (direct) methods of the kind used routinely with small-molecule crystals or maximum entropy and likelihood techniques. Such possibilities would allow a greatly increased rate of solving protein crystal structures. Additionally, the quality of the final model would be improved by the use of data sets which could be considered nearly *ideal*.

APPENDIX

Considerations of possible instrument configurations for ultra-short wavelengths at ESRF

The choice of operational wavelength in this range is determined by the need to maximize the detector absorption efficiency coupled with a high brilliance at that wavelength. The choice of wavelength is therefore governed by the barium K edge ($\lambda = 0.3310$ Å) for use of the image plate in this wavelength range, and the caesium and iodine K edges ($\lambda = 0.3445$ and 0.3738 Å respectively) for use of the caesium iodide-coated charge-coupled device. An operational wavelength of 0.33 Å is appropriate for native data. A second idea is the use of the K edges of Pt ($\lambda = 0.1582$ Å), Au ($\lambda = 0.1534$ Å) and Hg ($\lambda = 0.1492$ Å) for multi-wavelength anomalous-dispersion effects in a regime where absorption correction effects are effectively absent as a source of systematic error.

The use of these wavelengths requires long crystal-to-detector distances. It also means that a tight beam divergence is required in both the horizontal and vertical directions.

A.1. Radiation source

An undulator is required in a high β section to minimize the beam divergences of the emitted beam. The operational wavelength range for native data collection should be 0.32 to 0.36 Å and for multi-wavelength anomalous dispersion with high atomic number K edges in a tuning range of 0.149 to 0.158 Å. Hence, a third and a seventh harmonic serving these ranges can be provided if the fundamental is tunable between 0.96 and 1.11 Å (*i.e.* set by 3×0.32 and 3×0.36 Å and 7×0.149 and 7×0.158 Å). The fifth harmonic at ~0.2 Å can provide the reference wavelength for the multi-wavelength anomalous-dispersion work of these edges or alternatively the on-edge capability for the lanthanide K edges (*e.g.* Ho at 0.2229 Å).

A magnet design study is required to decide on the undulator period and magnetic field for machines like ESRF, APS or SPRING-8. Obviously the higher the machine energy the greater the tuning range can be although none of these machines will allow a fundamental at 0.3 Å. Use of a machine like PETRA would allow this.

A.2. Monochromator and mirror scheme

At high-energy machines where the circumference is large, the shield wall prevents the first optical element being put closer than 25 m or so. Hence, even with 0.1 mrad divergence angles in the horizontal and vertical the unfocused beam would be 2.5 $\times$ 2.5 mm^2, which is too large for a typical crystal

sample size. Focusing is therefore required. At these wavelengths (0.33–0.14 Å) a focusing mirror, even with a platinum coating, would need very fine grazing angles (1.5–0.86 mrad). At 25 m these angles would require mirror lengths of 1.7 and 2.9 m in order to pick up the full vertical aperture of 0.1 mrad. A full ray-tracing study is needed to assess the quality of focusing of a plane mirror bent to a cylinder for vertical focusing or of a cylindrical mirror bent to a toroid. It seems probable, taking due account of manufacturing tolerances, that the toroid would not be feasible here (owing to slope error) but the bent plane mirror might be.

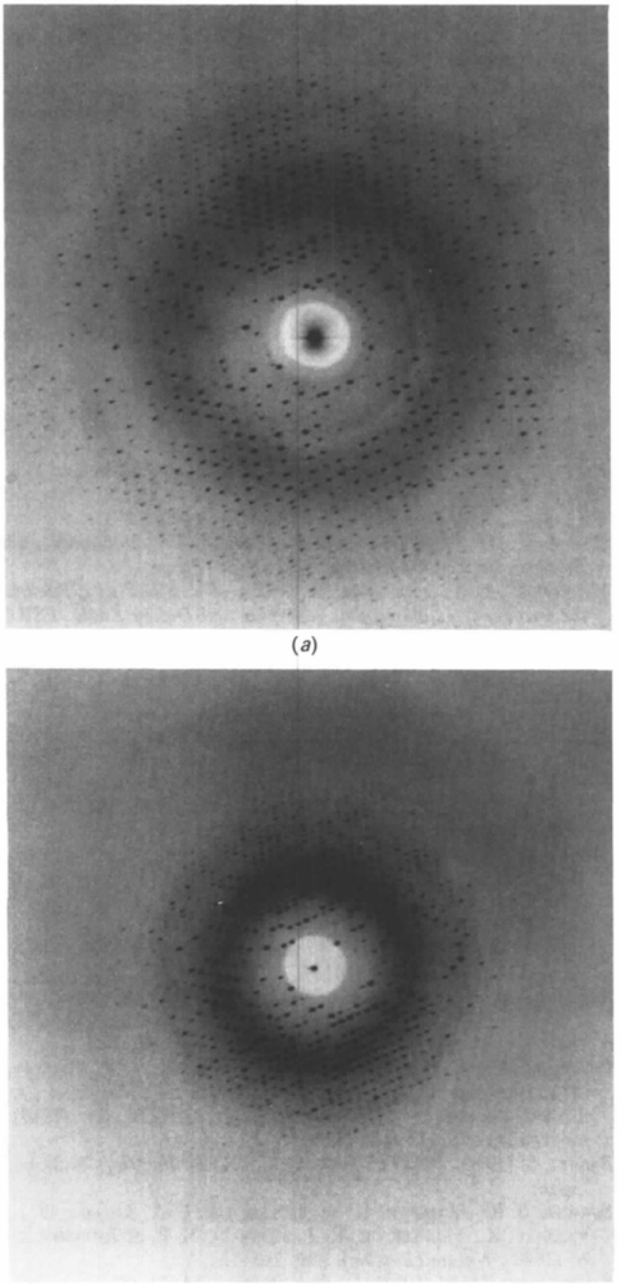

(*a*)

(*b*)

Fig. 4. Monochromatic rotation exposures, recorded on Fuji image plates and digitized on a Kodak scanner, using a lysozyme crystal. Rotation angle 1°. Wavelength of incident beam (*a*) 0.5 and (*b*) 0.3 Å. Crystal-to-plate distances in (*a*) and (*b*) were 300 mm. CHESS station F2 fed by a 24-pole multipole wiggler.

A horizontally focusing, bent triangle monochromator could be used to complement a vertical-focusing plane mirror and so produce a point focus. Unfortunately, this would restrict somewhat the ease with which the wavelength can be tuned. An alternative would be to provide the horizontal focusing with a second bent plane-mirror system set orthogonal to the vertical-focusing bent plane-mirror system. This is worth considering since the horizontal divergence angle is as small as the vertical on the undulator. This would then allow use of a monolithic double-crystal monochromator for ease of tuning. The practical feasibility of this depends upon the undulator magnet quality. Imperfections in the undulator magnet decrease the effectiveness of the higher harmonics and broaden the horizontal divergence angle. Hence, the 'double orthogonal mirror' system may be of ultimate interest on a machine like PETRA or TRISTAN operating at 14 and 30 GeV respectively. On ESRF it is probably better to examine the bent triangular monochromator option. In the following the calculation will determine the choice of monochromator crystal type and oblique cut angle. The rapidly tunable requirement may still be met by use of a symmetric cut triangle monochromator, 'overbent' (Arndt, Greenhough, Helliwell, Howard, Rule & Thompson, 1982) followed by a channel cut to select specific wavelengths in the band pass of the reflected beam from the symmetric cut bent triangle.

At $\lambda = 0.33$ Å, for Si(111) with $2d = 6.271$ Å, then $\theta = 3.016$, $2\theta = 6.032°$. A floor layout constraint would be for the largest horizontal deflection from the beam centreline, of the side scattering mode, to be about 1.5 m. A focusing length of $p' = 1.5/\sin 6.032°$ would be the maximum allowable, *i.e.* 14.3 m. Hence, with a mirror focusing 30 m to 30 m (*i.e.* 1:1) then the bent triangle would be placed at 45.7 m thus making a focusing ratio of 3.2:1. This would need an oblique cut of $\sim[(45.7 - 14.3)/(45.7 + 14.3)] \times 3.016° = 1.58°$ for a Guinier setting with $(\delta\lambda/\lambda)_{\text{corr}}$ zero.

The precise focal-spot size expected needs a full ray-tracing study taking account of undulator depth of source effects, electron source sizes and monochromator perfection. The monochromator acceptance for a 200 mm long crystal would be $[200 \times \sin(3.016° + 1.58°)]/45.7 = 0.36$ mrad, *i.e.* more than enough for a 0.1 mrad beam. The radius of curvature required would be 570 m provided by a deflection at the tip of the crystal of 70 μm.

At $\lambda = 0.14$ Å, for Si(111) with $2d = 6.271$ Å, then $\theta = 1.279$, $2\theta = 2.559°$. At 14.3 m from the monochromator, the displacement from the beam centreline will be 0.6 m. The oblique cut required now will be $[(45.7 - 14.3)/(45.7 + 14.3)] \times 1.279° = 0.67°$. The monochromator acceptance for a 200 mm long crystal would be $[200 \times \sin(1.279 + 0.67)]/45.7 = 0.15$ mrad, still enough to accept the undulator emission. The radius of curvature required will be 1345 m provided by a deflection at the tip of the crystal of 30 μm.

The alternative of an Si(220) monochromator would require more floor space, *e.g.* $\lambda = 0.33$ Å, Si(220), $2d = 3.8403$ Å, $\theta = 4.93$, $2\theta = 9.869°$. The displacement from the beamline centre will be 2.448 m at 14.3 m from the monochromator. If this is too much the focusing distance could be restricted to say 7 m thus reducing the displacement. This also increases the source demagnification to 7/45.7 from 14.3/45.7.

The Si(220) option at $\lambda = 0.14$ Å could be used at a focusing distance of 14 m and still be close to the beam centreline since $\theta = 2.089$, $2\theta = 4.178°$. Displacement from the beam centreline, 14.3 m from the monochromator, is now 1.05 m which is perfectly acceptable.

A.3. Detector

For 0.33 and 0.15 Å the ESRF CsI image intensifier system (Morse & Moy, personal communication) is of considerable interest. It should be possible to operate with an Al window at 0.15 Å (rather than Be). The image plate is also required on this beamline. Tests with both detector types at these wavelengths need to be made.

A.4. Pilot study

An extended pilot study of macromolecular crystal data collection at these wavelengths is planned.

JRH is grateful to J. Schneider (DESY) and M. Lehmann (Grenoble) for encouragement to pursue the ideas of wavelengths even shorter than 0.9 Å for macromolecular crystal data collection following lectures in Moscow (SR90) and Bordeaux (XVth World Congress) in 1990. JRH is also grateful to a variety of people for recent discussions on this topic particularly A. W. Thompson (EMBL/ESRF), P. Bosecke, M. Wulff and Å. Kvick (ESRF), K. S. Wilson (EMBL, Hamburg) and C. Nave (Daresbury). The University of Manchester is thanked for general support. MacCHESS is funded by NIH, USA, grant No. RR01646. Cambridge University Press is thanked for permission to reproduce extracts from the book by JRH entitled *Macromolecular Crystallography with Synchrotron Radiation* (ISBN 0521 334675).

References

ACHARYA, K. R., FRY, E., STUART, D., FOX, G., ROWLANDS, D. & BROWN, F. (1989). *Nature* (*London*), **337**, 709–716.

ANDERSSON, I., KNIGHT, S., SCHNEIDER, G., LINDQUIST, Y., LUNDQUIST, T., BRÄNDÉN, C. I. & LORIMER, G. H. (1989). *Nature* (*London*), **337**, 229–234.

ARNDT, U. W., GREENHOUGH, T. J., HELLIWELL, J. R., HOWARD, J. A. K., RULE, S. A. & THOMPSON, A. W. (1982). *Nature* (*London*), **298**, 835–838.

BARFORD, D. & JOHNSON, L. N. (1989). *Nature* (*London*), **340**, 609–616.

BLAKE, C. C. F. & PHILLIPS, D. C. (1962). In *Biological Effects at the Molecular Level*, IAEA Symposium. International Atomic Energy Authority: Vienna.

BOEL, E., BRADY, C., BRZOZOWSKI, A. M., DEREWENDA, Z., DODSON, G. G., JENSEN, V. J., PETERSEN, S. B., SWIFT, H., THIM, L. & WOLDIKE, H. F. (1990). *Biochemistry*, **29**, 624–629.

COLAPIETRO, M., CAPPUCCIO, G., MARCIANTE, C., PIFFERI, A., SPAGNA, R. S. & HELLIWELL, J. R. (1992). *J. Appl. Cryst.* **25**, 192–194.

GLOVER, I. D., HELLIWELL, J. R. & PAPIZ, M. Z. (1988). *Top. Curr. Chem.* **147**, 31–55.

GREENHOUGH, T. J. & HELLIWELL, J. R. (1982*a*). *J. Appl. Cryst.* **15**, 338–351.

GREENHOUGH, T. J. & HELLIWELL, J. R. (1982*b*). *J. Appl. Cryst.* **15**, 493–508.

HELLIWELL, J. R. (1984). *Rep. Prog. Phys.* **47**, 1403–1497.

HELLIWELL, J. R. (1988). *J. Cryst. Growth*, **90**, 259–272.

HELLIWELL, J. R. (1989). *Phys. World*, (January), 29–32.

HELLIWELL, J. R. (1992). *Macromolecular Crystallography with Synchrotron Radiation*. Cambridge Univ. Press.

HELLIWELL, J. R. & FOURME, R. (1983). *The ESRF as a Facility for Protein Crystallography: a Report and Design Study*. ESRP Report. CERN, Geneva.

HELLIWELL, J. R., PAPIZ, M. Z., GLOVER, I. D., HABASH, J., THOMPSON, A. W., MOORE, P. R., HARRIS, N., CROFT, D. & PANTOS, E. (1986). *Nucl. Instrum. Methods*, A**246**, 617–623.

HELLIWELL, J. R., PAPIZ, M. Z., MOORE, P. R. & THOMPSON, A. W. (1984). *Daresbury Study Weekend Proceedings*, DL/SCI/R22, pp. 123–127. Warrington: SERC Daresbury Laboratory.

HENDERSON, R. (1990). *Proc. R. Soc. London Ser. B*, **241**, 6–8.

HOPE, H. (1988). *Acta Cryst.* B**44**, 22–26.

HOUGH, E., HANSEN, L. K., BIRKNES, B., JYNGE, K., HANSEN, S., HORDVIK, A., LITTLE, C., DODSON, E. & DEREWENDA, Z. (1989). *Nature* (*London*), **338**, 357–360.

LESLIE, A. W. (1990). *J. Mol. Biol.* **213**, 167–186.

LESLIE, A. W., MOODY, P. C. E. & SHAW, W. (1988). *Proc. Natl Acad. Sci. USA*, **85**, 4133–4137.

LIDDINGTON, R. C., YAN, Y., MOULAI, J., SAHLI, R., BENJAMIN, T. I. & HARRISON, S. C. (1991). *Nature* (*London*), **354**, 278–284.

OIKONOMAKOS, N. G., JOHNSON, L. N., ACHARYA, K. R., STUART, D. I., BARFORD, D., HAJDU, J., VARVILL, K. M., MELPIDOU, A. E., PAPAGEORGIOU, T., GROVES, D. J. & PALM, D. (1987). *Biochemistry*, **26**, 8381–8389.

SASAKI, S. (1990). Report 90-16. KEK, Photon Factory, Tsukuba, Japan.

SPRANG, S. R., ACHARYA, K. R., GOLDSMITH, E. J., STUART, D. I., VARVILL, K., FLETTERICK, R. J., MADSEN, N. B. & JOHNSON, L. N. (1988). *Nature* (*London*), **336**, 215–221.

STUHRMANN, H. B. (1978). *Q. Rev. Biophys.* **11**, 71–98.

TONG, L., DE VOS, A. M., MILBURN, M. V., JANCARIK, J., NOGUCHI, S., NISHIMURA, S., MIURA, K., OHTSUKA, E. & KIM, S.-H. (1989). *Nature* (*London*), **337**, 90–93.

WALLER, D. A. & LIDDINGTON, R. (1990). *Acta Cryst.* B**46**, 409–418.

ZACHARIASEN, W. H. (1945). *Theory of X-ray Diffraction in Crystals*. New York: John Wiley.